

# SkinCells: Sparse Skinning using Voronoi Cells

EGOR LARIONOV, IGOR SANTESTEBAN, and HSIAO-YU CHEN, Meta Reality Labs, USA

GENE WEI-CHIN LIN, Meta Reality Labs, Canada

PHILIPP HERHOLZ, RYAN GOLDADE, and LADISLAV KAVAN, Meta Reality Labs, Switzerland

DOUG ROBLE and TUUR STUYCK, Meta Reality Labs, USA

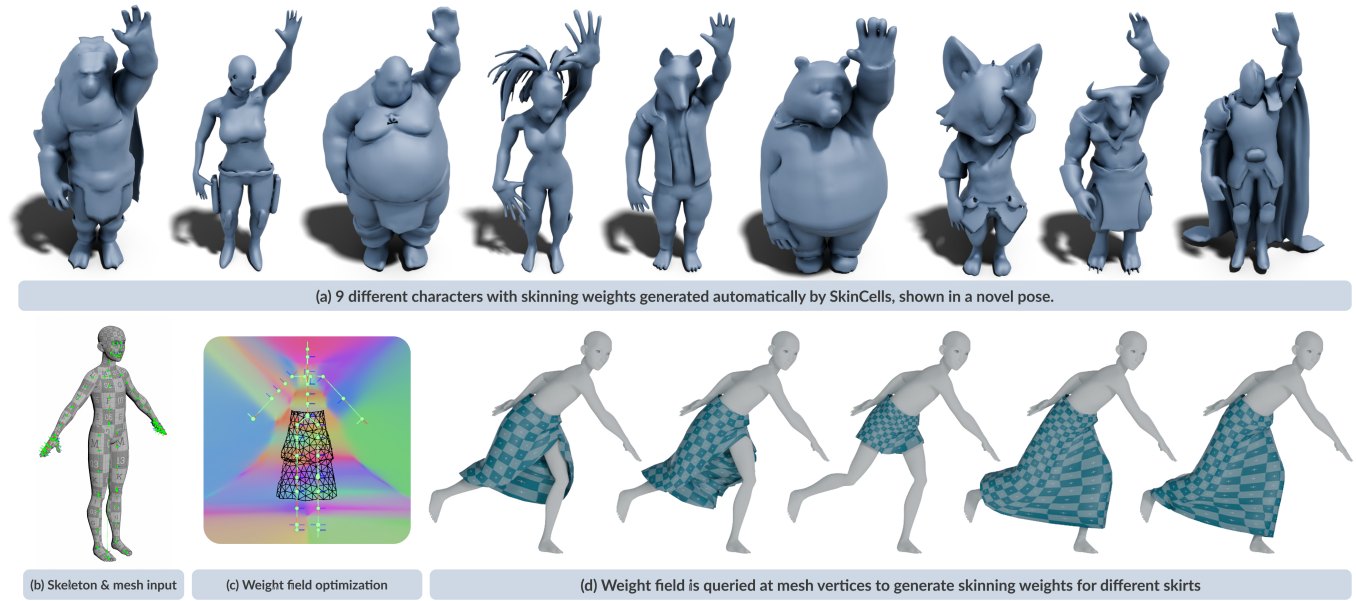


Fig. 1. SkinCells is a field-based framework for computing sparse skinning weights for characters and garments. By optimizing a weight field in canonical space (c), it binds meshes to a skeleton rig (b) while minimizing deformation artifacts. We demonstrate its effectiveness on nine characters using linear blend skinning (a) and five distinct skirt designs (d).

For decades, real-time skinning has been the cornerstone of character animation in visual effects and games. Despite its importance, the creation of animatable digital assets remains a labor-intensive manual process. Existing automated tools frequently struggle with intricate geometries, often necessitating significant manual refinement to reach production standards. We present a robust, fully automated method for generating high-quality skinning weights from a standard mesh and skeleton in a canonical A- or T-pose. Unlike traditional approaches, our framework offers direct sparsity controls to limit bone influences per vertex – a critical requirement for maintaining performance in large-scale mobile environments. Furthermore, we address the challenge of Level-of-Detail (LoD) management by optimizing weights within a continuous spatial volume rather than on discrete vertices. This allows a single optimization pass to be applied seamlessly across multiple asset resolutions and variations. Central to our approach is a novel parameterized family of functions, we call SkinCells. We demonstrate that our method consistently produces stable, high-quality results even in complex scenarios where standard biharmonic weight computations fail.

CCS Concepts: • **Computing methodologies** → **Animation**.

Authors' Contact Information: Egor Larionov, [elrnv@meta.com](mailto:elrnv@meta.com); Igor Santesteban, [isantesteban@meta.com](mailto:isantesteban@meta.com); Hsiao-yu Chen, [hsiao-yu@meta.com](mailto:hsiao-yu@meta.com), Meta Reality Labs, USA; Gene Wei-Chin Lin, [genelin@meta.com](mailto:genelin@meta.com), Meta Reality Labs, Vancouver, Canada; Philipp Herholz, [herholz@meta.com](mailto:herholz@meta.com); Ryan Goldade, [ryangoldade@meta.com](mailto:ryangoldade@meta.com); Ladislav Kavan, [lkavan@meta.com](mailto:lkavan@meta.com), Meta Reality Labs, Zurich, Switzerland; Doug Roble, [droble@meta.com](mailto:droble@meta.com); Tuur Stuyck, [tuur@meta.com](mailto:tuur@meta.com), Meta Reality Labs, Sausalito, CA, USA.

Additional Key Words and Phrases: character animation, cloth animation, skinning weights, level-of-detail

## 1 Introduction

Character animation has long been a cornerstone of graphics research, with a myriad of techniques developed to efficiently animate complex shapes. A popular family of methods called *skinning* [Jacobson et al. 2014] is widely adopted in visual effects, animation, and gaming industries. These methods allow for the efficient manipulation of character models by binding them to skeletal structures; assigning a set of weights (scalar values that typically sum to 1) to each vertex, indicating which skeleton bones the vertex should follow. This enables efficient real-time animation in interactive applications. Although automated skinning weight methods have been introduced, preparing these models for animation often still requires manual, labor-intensive processes. This is particularly true when dealing with complex characters that feature intricate details, accessories, and non-manifold geometries. In such cases, extensive manual refinement of automatically generated results is frequently necessary to achieve the desired level of quality.

Although physics-based simulations [Wang et al. 2020; Xu and Barbič 2016] and neural approaches [Yang et al. 2021] can offer a

more realistic alternative, they are too resource-intensive for real-time use, especially on mobile devices that may need to animate and render many characters and assets simultaneously. In these scenarios, most of the limited compute budget is typically allocated for rendering since research shows that appearance modeling is key to achieving visual realism, e.g. for animated fabrics [Aliaga et al. 2015].

The recent surge in generative AI models for automatically generating content at-scale highlights the growing need for dependable, high-quality, and automatic solutions that can efficiently produce animation-ready assets. While there is a large focus on mesh generation techniques [Gao et al. 2025; Sarafianos et al. 2025; Wei et al. 2024; Zhang et al. 2024], these methods often omit generating accompanying rigs with skinning weights. To fully automate and democratize digital content generation, it is essential to address the full end-to-end process of rigged asset generation [Guo et al. 2025; Liu et al. 2025] and skinning weight computation.

In this work, we focus on automatic skinning weight computation, where the character mesh and a compatible skeleton have already been determined. Existing automated techniques for skinning weight computation, while innovative, often struggle with complex mesh topologies, details and LOD hierarchies found in production models. In response to these challenges, we introduce a novel approach for computing weights using a weight field representation designed to optimize skinning weights by leveraging randomly sampled character poses. This method reduces deformation artifacts and results in a weight field that is independent of mesh topology, directly providing weights for all LOD levels. Although one could resort to weight transfer across different resolutions, this requires additional steps and we demonstrate that transferring weights produces subpar results.

Similar to diffuse weights, a widely used technique for skinning 3D Gaussian Splatting (3DGS) [Kerbl et al. 2023] representations of humans [Li et al. 2024; Lin et al. 2022], our weight field representation is defined in ambient 3D space, allowing for immediate weight transfer across different models of the same character (e.g. to a high-fidelity model or a 3DGS representation). Our weight representation is also compact, storing all parameters in single precision floats takes just 21 KB, whereas storing 4 weights per vertex along with corresponding weight indices can take up 11x more space in our experiments.

Our approach prioritizes robustness and high-quality deformations while maintaining sparse weight distributions, ensuring that the number of bone influences for each vertex can be constrained. This results in a highly efficient system capable of supporting numerous unique characters on devices with limited computational resources. While prior work [Dionne and Lasa 2013] has explored sparsity using falloffs to limit bone influences, it does not provide any numerical guarantees or controls on sparsity and optimizing for truly sparse weights while retaining smoothness has been acknowledged as an open problem [Jacobson et al. 2014]. We propose an optimization formulation that incorporates a novel set of goal functions to optimize skinning weights with the following desirable properties: smooth weights, ensuring a natural and continuous deformation of the mesh; sparsity for efficiency, reducing computational overhead by minimizing the number of non-zero weights,

essential for efficient asset creation, especially for performance-sensitive applications like mobile platforms [Diamant and Simantov 2010]; and an additional location objective, preventing trivial solutions where the mesh is not influenced by the skeleton, thereby maintaining a meaningful relationship between the two.

Our comprehensive evaluations reveal that our method strikes a balance between robustness and quality, generating high-quality weights while maintaining robustness. In contrast, comparative works often compromise on one aspect for the other, either prioritizing quality at the expense of robustness or vice versa. Our approach offers a streamlined solution for automatic skinning weight computation with sparsity enforcement and easy LOD weight generation, significantly reducing the time and effort required in the animation pipeline by offering a robust solution.

Compared to prior work, we provide the following contributions:

- Controllable enforcement for the limit on the number of bone influences per vertex, which we refer to as sparsity.
- A system that integrates with level-of-detail asset generation by optimizing spatially varying weights, applicable to all detail levels through a single optimization process.
- A novel optimizable weight field formulation inspired by Voronoi cell structures that is intrinsically diffuse, can enforce sparsity and works well for generating cloth and character skinning fields.
- A novel set of loss functions to produce optimal skinning weights. (i) A *sparsity objective* to penalize weight distributions with more than a set number of nonzero weights per point. (ii) A *smoothness objective* based on the Delta-Mush [Mancewicz et al. 2014] method. (iii) A *spring-based location objective* ensuring that the mesh follows the skeleton.

## 2 Related Work

*Skinning.* Deforming a mesh through an underlying skeleton structure (i.e. skinning), is a longstanding, foundational approach for computer graphics animation [Magenat-Thalmann et al. 1989]. Recent research has focused on enhancing skinning accuracy through various techniques. Considerable attention has been given to runtime improvements to skinning. Dual quaternions [Kavan et al. 2007] improved rotation blending, and physics-based methods [Komaritzan and Botsch 2018] introduced physics priors into skinning. Other studies have explored the addition of second-order motions to standard skinning [Benckekroun et al. 2023; Kalyasundaram et al. 2022; Rohmer et al. 2021; Zhang et al. 2020]. To simplify the process of editing skinning weights some works proposed to use splines [Bang and Lee 2018], while we aim to automate this process altogether. In some cases, optimal mesh deformations are known a priori, allowing algorithms [Le and Deng 2012] to find optimal rigging configurations to fit them. Additional efforts have been made to improve efficiency for real-time high-quality deformations across multiple levels of detail (LOD) [Zheng and Barbic 2024], highlighting the importance of supporting LOD in animation. A current trend in machine learning involves optimizing weight fields by learning from physical models [Modi et al. 2024] or directly from data [Lin et al. 2022; Liu et al. 2019; Saito et al. 2021]. In either case, weight

fields make a natural tool for building topology independent skinning with a natural support for LOD. Another approach is to predict vertex weights directly using neural models [Mosella-Montoro and Ruiz-Hidalgo 2022], and some propose to predict skinning weights and hierarchical skeletons simultaneously [Song et al. 2025; Xu et al. 2020b]. Another interesting line of work facilitates skin weight transfer [Abdrashitov et al. 2023; Cao and Mukai 2024], which leverages template rigs to animate new characters or clothing.

*Skinning Weights.* In this work, we focus on the automatic computation of skinning weights for a given skeleton rig with an emphasis on sparsity. A straightforward approach to computing skeleton-based weights assigns each mesh vertex a value inversely proportional to its distance from the skeleton. To limit the influence of distant bones, this value can be further attenuated with an exponent. This technique is commonly known as proximity-based weighting. While intuitive, this approach is blind to mesh topology and can produce artifacts where one limb can erroneously affect another if it is positioned close together (e.g. fingers on a hand) in a canonical pose. To mitigate this, much effort has been dedicated to inject the mesh topology in the weight computation process. Diffusing bone influences to the surface mesh [Baran and Popović 2007] helps resolve this artifact. Other works including *bone glow* [Wareham and Lasenby 2008], *quasi-harmonic* [Wang and Solomon 2021] and *biharmonic* [Dodik et al. 2025; Jacobson et al. 2011] skinning further improve the quality of generated weights. However, an important criteria for efficient skinning is maintaining sparsity of generated weights. While some methods [Landreneau and Schaefer 2010; Le and Deng 2013] propose a post-process to compress a given set of skinning weights, others [Thiery and Eisemann 2018] propose to enforce sparsity as a pre-process, which selects a fixed and potentially suboptimal configuration a priori. In contrast, our method has a built-in control for enforcing sparsity, which is optimized along with smoothness and locality penalties avoiding local minima especially within complex topologies. Prior work [Kavan and Sorkine 2012; Thiery and Eisemann 2018] discovered the importance of penalizing deformation artifacts in sampled poses – rather than enforcing intrinsic properties like weight smoothness. Our method builds on this idea giving the algorithm the opportunity to find elusive optimal weight distributions. Other works [Ma et al. 2024] also leveraged the Voronoi nature of influence regions for building an interactive skinning tool. For a more comprehensive overview of prior work, see the course notes on skinning [Jacobson et al. 2014].

*Animation.* Physics-based simulation of soft tissues in characters [Kim and Eberle 2022; Macklin and Muller 2021; Smith et al. 2018] and clothing [Baraff and Witkin 1998; Choi and Ko 2002; Stuyck 2022] has been a long standing research field within computer graphics with many significant advances. It is an established solution for producing realistic body and garment behavior. An alternative to modeling pose-dependent deformations for a rigged body is to apply pose-dependent correctives. Although efficient, such a model needs to be manually set up or trained from captured data [Allen et al. 2006; Xu et al. 2020a].

In recent years, the field has shown interest in learning-based solutions and skinning serves as the basis for many of these methods [Bertiche et al. 2022; Halimi et al. 2022; Santesteban et al. 2019,

2022; Stuyck et al. 2025]. These methods are conditioned on the body skeleton pose and predict deformations in a canonical pose, which gets posed to world space using skinning. This greatly facilitates learning as it provides a unified canonical space for easier learning. Early work by Santesteban et al. [2019] proposed a data-driven approach to learning cloth dynamics, which was later extended to a self-supervised setting [Bertiche et al. 2022; Santesteban et al. 2022] where cloth deformations are learned from physics supervision directly, without the need for simulated training data.

*Voronoi fields.* Feng et al. [2023] introduced a topology optimization algorithm that utilizes a differentiable and generalized Voronoi representation, enabling the evolution of cellular structures as continuous fields and extended this to accommodate anisotropic cells, free boundaries, and functionally-graded cellular structures. Herholz et al. [2017] compute intrinsic Voronoi diagrams on surfaces using heat diffusion. As an application they compute skinning weights using Sibson coordinates. Based on a sparse set of point handles, weights for a specific vertex are computed by adding it to the diagram and analyzing how much area the new cell took from cells of the initial diagram.

### 3 Method

Inspired by Voronoi diagrams, we similarly employ an implicit weight field function to automatically generate skinning weights. We begin by introducing the concepts of skinning (Sec. 3.1) and Voronoi cells (Sec. 3.2), laying the groundwork for the novel aspects of our method, which are presented in greater detail in the following sections.

#### 3.1 Skinning

Skinning is a fundamental technique in character animation used to deform a mesh according to an underlying skeletal structure, enabling realistic and controllable animation. One of the simplest and most widely adopted skinning techniques is Linear Blend Skinning (LBS) [Jacobson et al. 2014; Magnenat-Thalmann et al. 1989]. In LBS, each vertex of the mesh is moved by a weighted combination of bone transformations. Formally, the deformed position of a vertex  $\mathbf{x}$  is computed as

$$\text{LBS}(\mathbf{x}; \mathbf{w}, \mathbf{T}) = \sum_{j=1}^n \mathbf{w}_j \mathbf{T}_j \mathbf{x}, \quad \text{where} \quad \sum_j \mathbf{w}_j = 1, \quad (1)$$

where  $n$  is the number of joints,  $\mathbf{w} \in \mathbb{R}^n$  are the skinning weights and  $\mathbf{T}_j \in \mathbb{R}^{4 \times 4}$  are the affine transforms of the joints in the current pose. This linear interpolation of transformations is computationally efficient and easy to implement, making LBS the *de facto* standard in real-time applications. However, LBS suffers from several well-known artifacts, including volume loss near joints and unnatural collapsing or candy-wrapper effects during extreme bending. These limitations motivated more advanced skinning models, such as dual quaternion skinning [Kavan et al. 2007] and pose-space deformation [Lewis et al. 2000] techniques, which aim to preserve volume and improve realism. However, these more complex techniques are applied at run-time, negatively impacting performance. We observe

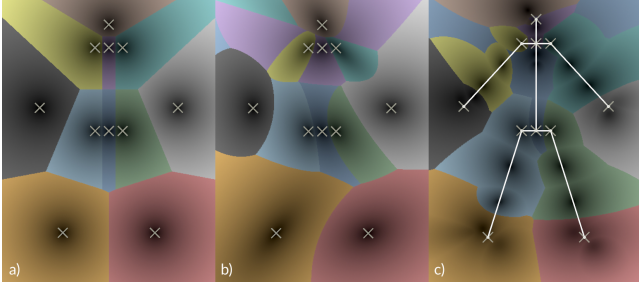


Fig. 2. A distance field (black at 0) for 11 regions (colored for clarity) marked with  $\times$ . (a) shows the field with uniformly shaped cells. (b) shows cells with randomly sampled  $\mathbf{s}$  and  $\mathbf{R}$  per site. In (c), each region is split into multiple sites sampled along the bones of the outlined skeleton.

that, by leveraging the joint limits of the rig, we can optimize skinning weights as a pre-process using pose samples within these constraints to effectively reduce unnatural distortions and thus enhance overall deformation quality without incurring additional run-time costs. Alternatively, poses can be sampled from motion capture or animated sequences but we found that randomly sampled poses produce comparable results while requiring fewer resources.

### 3.2 Voronoi Cells

Voronoi diagrams are a construct in computational geometry that partition a given space based on proximity to a discrete set of points. Given a set  $\{\mathbf{p}_1, \mathbf{p}_2, \dots, \mathbf{p}_n\}$  of distinct sites in a metric space (in our case  $\mathbb{R}^3$ ), the Voronoi diagram divides the space into  $n$  regions, such that each region  $V_D(\mathbf{p}_j) \subset \mathbb{R}^3$  consists of all points in the space that have  $\mathbf{p}_j$  as their closest neighbour. Formally, the Voronoi cell for site  $\mathbf{p}_j$  is defined as  $V_D(\mathbf{p}_j) = \{\mathbf{x} \in \mathbb{R}^3 : d(\mathbf{x}, \mathbf{p}_j) \leq d(\mathbf{x}, \mathbf{p}_k) \forall k \neq j\}$ , where  $d : \mathbb{R}^3 \rightarrow \mathbb{R}$  is a distance function.

Voronoi cells for constructing skinning weights follows the same motivations as traditional techniques; compute weights based on proximity to the nearest bone. This concept is also seen in diffuse skinning fields [Lin et al. 2022; Saito et al. 2021], which resemble Voronoi cells with segment-shaped sites. By leveraging the link between heat diffusion and Voronoi diagrams, we can compute distance fields that mimic diffusion behavior [Herholz et al. 2017].

### 3.3 Skin Cells

Inspired by Voronoi cells, we propose a novel formulation called *skin cells*. Voronoi diagrams create discrete boundaries of non-overlapping regions. Instead, skin cells introduces overlapping cells to control sparsity of the resulting field by adjusting the overlap of a predetermined number of cells. Each skin cell defines a local skinning weight field  $w(\mathbf{x}; S_j)$  around each joint of the input skeleton, where  $S_j$  is a set of parameters optimized per joint. We then combine these local fields to define the global skinning weight field as

$$\mathbf{w}(\mathbf{x}) = [\mathbf{w}_1(\mathbf{x}), \dots, \mathbf{w}_n(\mathbf{x})], \quad \text{where} \quad \mathbf{w}_i(\mathbf{x}) = \frac{w(\mathbf{x}; S_i)}{\sum_j w(\mathbf{x}; S_j)}. \quad (2)$$

Since the field  $\mathbf{w}(\mathbf{x})$  is continuous and agnostic of the mesh topology, it can be easily applied to compute the skinning weights of multiple LoDs of the same mesh, or meshes that represent similar

objects (e.g., reuse the same field to skin different types of skirts). While skinning weight fields have been extensively explored [Bhatnagar et al. 2020; Lin et al. 2022; Saito et al. 2021; Santesteban et al. 2021], our method provides a more compact parameterization where locality and sparsity are easily enforced.

We first introduce our approach to model parametric distance fields by extending the Voronoi cell formulation, then we describe how to extract sparse skinning weights from the skin cell distances.

*Distance function.* We propose a Mahalanobis distance metric from a point  $\mathbf{x}$  to a site  $\mathbf{p}$

$$d(\mathbf{x}, \mathbf{p}; \mathbf{F}) := \sqrt{(\mathbf{x} - \mathbf{p})^T \mathbf{F}^T \mathbf{F} (\mathbf{x} - \mathbf{p})},$$

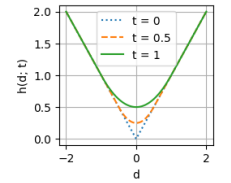
where  $\mathbf{F} \in \mathbb{R}^{3 \times 3}$  is the deformation gradient of the site, i.e.  $\mathbf{F} = \text{diag}(\mathbf{s})\mathbf{R}$  with  $\mathbf{s} \in \mathbb{R}^3$  and  $\mathbf{R} \in \text{SO}(3)$ . Note that  $d$  is well defined since  $\mathbf{F}^T \mathbf{F}$  is symmetric positive definite (SPD). This adaptation enables the metric to be scaled and rotated, allowing for a more nuanced and rig-aware weight distribution as shown in Fig. 2.

*Distance field.* To improve the ability to model complex distance fields, we allow the skin cells to have more than one site. We define the set of sites as  $P_j = \{P_{j,1}, \dots, P_{j,m}\}$  where  $P_{j,k}$  are the site parameters including the site center  $\mathbf{p}$ , the scale  $\mathbf{s}$ , and the rotation  $\mathbf{R}$ , and  $m$  is the user-specified number of sites. In our experiments, we find that  $m = 6$  is sufficient to strike a balance between performance and expressibility for our examples, although more complex meshes may benefit from a higher  $m$ . The distance to the skin cell  $j$  is then defined as the distance to the closest site in  $P_j$

$$d(\mathbf{x}; P_j) = \min_k \{h(d(\mathbf{x}; P_{j,k}), t_{j,k})\},$$

where  $h$  is a function that modulates the contribution of each site to the distance field, controlled by an additional per-site parameter  $t_{j,k} \in \mathbb{R}$ . Inspired by the Huber loss [Huber 1992], we define  $h$  as shown in the inset with

$$h(d; t) = \begin{cases} \frac{1}{2} \left( \frac{|d|^2}{t} + t \right) & |d| < t \\ |d| & \text{otherwise.} \end{cases}$$



*Weight field.* To extract valid skinning weights from the distance field, the distances must now be transformed into the range  $[0, 1]$  with 0 being on the cell boundary and 1 at the site locations. We must also allow more than one nonzero weight per point in space, normalized to ensure weights add up to 1. To do this, first we define the pointwise sorting for these distances as

$$D(\mathbf{x}) = \text{sort}[d(\mathbf{x}; P_j)]_{j=1}^n,$$

where  $D(\mathbf{x})_1$ , the first value, is the distance to the closest joint. Finally, we define the skinning weight field for each skin cell as

$$w(\mathbf{x}; S_j) = \left( \frac{\max(c_j, D(\mathbf{x})_l - d(\mathbf{x}; P_j))}{d(\mathbf{x}; P_j)} \right)^{r_j} \quad (3)$$

where  $S_j = \{P_j, c_j, r_j\}$  are the skin cell parameters including additional parameters  $r_j, c_j$  that control the falloff and sparsity of the resulting field, and  $l$  is the number of non-zero weights set by the user. Once the skin cell of each joint is defined, we compute the normalized skinning weights for a point  $\mathbf{x}$  following Eq. 2. Note that

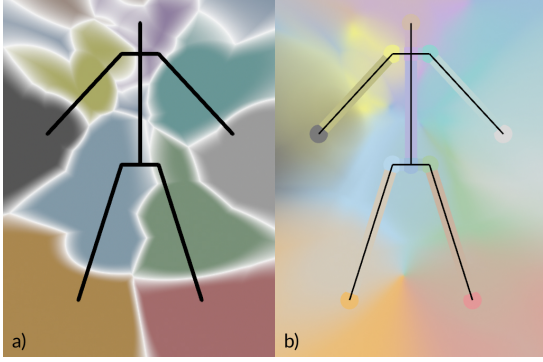


Fig. 3. (a) shows the unnormalized weight field  $\mathbf{w}$  for  $l = 1$  where each region  $j$  is uniquely colored and white indicates a zero value. (b) plots the normalized Voronoi field with  $l = 3$  indicating that there are at most 3 nonzero weights for each point  $\mathbf{x}$ . The outline of the source skeleton is shown in black for clarity.

Eq. 3 reduces to the standard proximity-based weight field when the numerator is set to a constant, which can be achieved for sufficiently large  $c_j$ .

*Sparsity.* Examining the fractional term in Eq. 3 we can see that for  $c_j = 0$ , we have  $\|\mathbf{w}(\mathbf{x})\|_0 \leq l$  for all  $\mathbf{x}$  where  $\mathbf{w}$  is well defined, where  $\|\cdot\|_0$  is the  $l_0$ -“norm” counting nonzeros of a vector. This guarantees that for any set of parameters, setting  $c_j = 0$  for all  $j$  produces a guaranteed sparse field with  $\mathbf{w}(\mathbf{x})$  having at most  $l$  nonzeros for any  $\mathbf{x}$ . The purpose of  $c_j$  as an optimizable parameter is to relax the sparsity constraint temporarily to enable non-zero objective gradients in distant points during optimization. Fig. 3a shows the unnormalized value of  $\mathbf{w}$  for  $l = 1$ , where the boundary between the cells is clearly visible. Fig. 3b plots  $\mathbf{w}$  for  $l = 3$  initialized using a toy skeleton and the scheme described in the next section.

### 3.4 Initialization

To improve parameter optimization convergence, we must first distribute the sites for each skin cell. The skin cell sites are initialized by sampling along the hierarchical skeleton rig, composed of 3D points representing joints and connecting segments representing bones. Each joint corresponds to a single skin cell with  $m$  sites. For each joint with exactly one child, we sample  $m$  points along the bone. For joints with multiple children we randomly sample the *convex hull* containing all the immediate child joints. Finally, the sites associated to leaf joints (like ends of fingers or feet) are sampled in a small 0.5 mm radius around the joint. The remaining parameters are sampled from a uniform distribution. Rotations  $\mathbf{R}$  and scales  $s$  can be sampled separately from a uniform distribution, or alternatively, the lower triangular entries of  $\mathbf{F}$  can be randomly sampled directly spanning the space of SPD matrices  $\mathbf{F}^T \mathbf{F}$ . Parameters  $c$ ,  $t$ ,  $r$ , and are uniformly sampled from  $\exp(\text{Uniform}(-0.05, 0.05))$ , where. In practice, to enforce strict positivity, we apply the exponential on the optimized parameters before passing them to Eq. 2.

### 3.5 Loss Formulation

An optimal set of weights for a given mesh and skeleton should minimize the amount of mesh deformation caused by skeleton poses, while preserving the overall *intent* of the pose. In other words, the mesh should follow the skeleton while preserving a desired level of smoothness. Furthermore, we aim to produce skinning weights of no more than  $l$ -many bone influences per vertex. This motivates the three losses we propose to minimize (see Sec. 3.6) over skin cell parameters  $S_j$  to achieve the best possible skinning weight distribution.

*Smoothness loss.* Inspired by traditional graphics techniques, we reformulate a popular method for smoothing deformations, called DeltaMush [Mancewicz et al. 2014], into a form that can easily fit our optimization problem. The method was originally designed as a runtime filter to smooth away artifacts introduced by skinning while retaining surface details present in the rest geometry. This is done by adding the delta produced by smoothing in rest configuration, to the result of smoothing the deformed configuration. This is performed in the coordinate frame of the surface to preserve as much detail as possible. The method relies on Laplacian smoothing, an iterative procedure of repeated applications of the discrete linear Laplacian  $\mathbf{L} : \mathbb{R}^{3V} \rightarrow \mathbb{R}^{3V}$  on  $V$  mesh vertex positions.

We represent a mesh configuration using a matrix of stacked vertex positions. Specifically, we use  $\bar{\mathbf{X}} \in \mathbb{R}^{3V}$  to denote the rest configuration of the mesh and  $\mathbf{X} = \text{LBS}(\bar{\mathbf{X}}; \mathbf{w}, \mathbf{T})$  the deformed configuration after skinning, as described in Eq. 1. A single iteration of the Laplacian operator  $\mathbf{L}$  is sufficient for our purposes, so the smoothed configuration can be defined as  $\mathbf{X}' = \mathbf{X} + \lambda_{\text{DM}} \mathbf{L} \mathbf{X}$ , where  $\lambda_{\text{DM}}$  is the smoothing coefficient that is later used to scale the resulting loss component. For brevity, we denote the change of basis rotation that maps vectors from  $\bar{\mathbf{X}}$  to the deformed configuration  $\mathbf{X}$  as  $\mathcal{B}$ . DeltaMush can then be written as  $\mathbf{X}_D = \mathcal{B}(\bar{\mathbf{X}} - \bar{\mathbf{X}}') + \mathbf{X}'$ , which reduces to  $\mathbf{X}_D = \mathbf{X} + \lambda_{\text{DM}}(\mathbf{L}(\mathbf{X}) - \mathcal{B}\mathbf{L}(\bar{\mathbf{X}}))$ . This expression indicates that the displacement produced by DeltaMush can be defined as  $\lambda_{\text{DM}}(\mathbf{L}(\mathbf{X}) - \mathcal{B}\mathbf{L}(\bar{\mathbf{X}}))$ . Instead of applying this displacement at run-time, we use it to formulate the following loss that encourages smooth deformations while preserving surface details

$$\mathcal{L}_{\text{DM}} = \|\mathbf{L}(\mathbf{X}) - \mathcal{B}\mathbf{L}(\bar{\mathbf{X}})\|_2^2. \quad (4)$$

*Location loss.* The minimizer of just Eq. 4 is the rest configuration  $\mathbf{X}$  which does not follow the intended skeleton animation. This means that minimizing a smoothness loss alone will not produce a useful weight distribution. This phenomenon has been previously addressed by adding an orthogonality loss on the weight distribution [Modi et al. 2024]. However, in our case it is useful to preserve the weight field correspondences to bones, which makes the result editable and controllable in downstream applications. To ensure that the mesh follows the skeleton, we attach springs from each vertex on the mesh to the closest point on the skeleton. We prune any springs not orthogonal to the connecting bone and that intersect the mesh in any way. Let  $\mathbf{d}_s : \mathbb{R}^{3V} \rightarrow \mathbb{R}^M$  denote the distances of all  $M$  valid springs for a given mesh configuration. The resulting



Fig. 4. Three examples of uniformly sampled poses used for further optimizing  $\mathbf{w}$  by updating  $S$  to minimize  $\mathcal{L}$ .

loss can then be written as

$$\mathcal{L}_{\text{loc}} = \left\| \frac{\mathbf{d}_s(\mathbf{X}) - \mathbf{d}_s(\bar{\mathbf{X}})}{\mathbf{d}_s(\bar{\mathbf{X}}) + 10^{-2}} \right\|_2^2, \quad (5)$$

where the denominator (computed coordinate-wise) ensures that far away vertices are not constrained as much as vertices close to the skeleton as one would expect on a real body. The  $10^{-2}$  stabilizer appearing in the denominator assumes units to be in cm.

*Sparsity loss.* Finally, we encourage sparsity using a loss that indirectly penalizes artifacts caused by clamping the lowest  $n - l$  weights in  $\mathbf{w}$  to 0. Formally, if we define  $\text{Top}[l] : \mathbb{R}^n \rightarrow \mathbb{R}^n$  to set the lowest  $n - l$  weights to zero such that  $\|\text{Top}[l](\mathbf{w})\|_0 \leq l$ , then our sparsity loss can be written as

$$\mathcal{L}_{\text{sp}} = \|\text{LBS}(\bar{\mathbf{X}}; \mathbf{w}) - \text{LBS}(\bar{\mathbf{X}}; \text{Top}[l](\mathbf{w}))\|_2^2. \quad (6)$$

With positive  $c_j$  the field function in Eq. 3 allows joints to have some small influence on far away vertices. This produces a non-zero gradient, even for bones that are farther away giving the optimization a better chance at recovering from a poor initialization.

The final loss is a weighted sum of these three losses

$$\mathcal{L} = \lambda_{\text{DM}} \mathcal{L}_{\text{DM}} + \lambda_{\text{loc}} \mathcal{L}_{\text{loc}} + \lambda_{\text{sp}} \mathcal{L}_{\text{sp}}, \quad (7)$$

where we choose  $\lambda_{\text{DM}} = \lambda_{\text{sp}} = 1$ , and  $\lambda_{\text{loc}} = 6000$  for all our experiments (unless otherwise stated). We found that a large range of parameters generates reasonable results. For details, refer to Sec. 4 under *Smoothness and control trade-off*. When skinning fine meshes, it may be necessary to prioritize sparsity to avoid tearing artifacts. For instance we used  $\lambda_{\text{sp}} = 1000$  for the example in Fig. 10. Note that while the space of parameters is scale independent since we sample distances on the mesh scaled to a unit box, the loss Eq. 7 remains scale sensitive.

### 3.6 Optimization

Once the weight field  $\mathbf{w}$  is initialized as described in Sec. 3.4, we optimize the skin cell parameters  $S = S_1, \dots, S_n$  by evaluating the loss  $\mathcal{L}$  at randomly sampled poses. Taking a manually defined range of motion for each joint on a hierarchical rig, we uniformly sample joint angles  $\theta$  to produce random (and usually non-physical) poses as shown in Fig. 4. Alternatively, one could sample from animated sequences when available. We define the joint transform

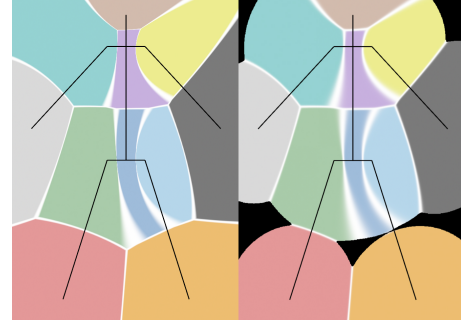


Fig. 5. The Voronoi field produced by our method (left) does not suffer from the same numerical instability resulting from softmax used by prior methods (right) where black represents NaN regions [Feng et al. 2023].

$\mathbf{J} : \mathbb{R}^{3n} \rightarrow \mathbb{R}^{n \times 4 \times 4}$ , which transforms local joint angles to world space transforms  $\mathbf{T}$ , which gives the final optimization problem:

$$\arg \min_S \mathcal{L}(\mathbf{w}(S), \mathbf{J}(\theta)). \quad (8)$$

## 4 Results

We implement the optimization problem defined by Eq. 8 in PyTorch using the Adam optimizer. We sample 20 poses per batch and set the learning rate to  $10^{-3}$ . For all experiments we set the maximum number of bone influences  $l = 4$ , however larger values can be used to obtain smoother results allowing more joints to affect the motion of each vertex.

*Voronoi field stability.* Prior work has employed smooth Voronoi fields [Feng et al. 2023] to represent differentiable Voronoi diagrams for representing cellular structures by applying softmax on the distance field, thereby generating a normalized and smooth field with a controllable falloff. However, this method runs into numerical instabilities even for moderately sized exponents, which is especially noticeable as distance values increase. In Fig. 5, we show how our field function compares to the state-of-the-art differentiable model proposed by Feng et al. [2023] for sites seeded using a 2D toy skeleton. The rational expression used in softmax divides small floating point numbers for larger distances. This is exacerbated when using a larger exponent to achieve a sharper falloff, which results in numerical instability shown by the black regions in the figure.

*Smoothness and control trade-off.* Our formulation has a unique property that users can adjust the trade-off between smoothness of the resulting skinning and control (how closely the mesh follows the underlying rig) by adjusting the  $\lambda_{\text{loc}}$  parameter. In Fig. 6 we show how increasing the  $\lambda_{\text{loc}}$  parameter results in deformations that more faithfully follow the underlying skeleton (e.g. in the leg of the character (middle)), while decreasing the parameter results in smoother deformation (e.g. the leg is smoother along the bends but loses volume (right)), compared to the rest shape (left).

*Timing results.* Optimizations were run for 1500 steps with 1024 randomly sampled poses batched at 16 poses per iteration. On an RTX A6000 GPU, in all tried examples the relative change in deformation became minimal within 1 minute, indicating convergence.

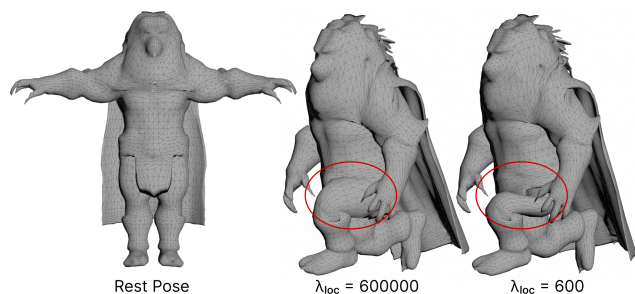


Fig. 6. The parameter  $\lambda_{loc}$  is increased (middle) on the lion character (model in rest pose on the left) to produce deformations more faithful to the underlying skeleton. Decreasing  $\lambda_{loc}$  (right) produces a smoother fold where the leg bends, albeit with more volume loss.

#### 4.1 Comparisons

We compare our method to two main approaches, a proximity-based weight mapping and bounded biharmonic weights (BBW) [Jacobson et al. 2011]. We demonstrate that while the proximity-based method is robust, results are not always sufficient and can lead to artifacts. On the other hand, BBW produce high quality results but lack robustness (due to the dependency on a tetrahedralization step) and sparsity controls. We show that our method provides a robust solution to obtaining high quality weights.

*Character skinning.* We apply our method to a set of 40 artist generated character models with associated skeleton rigs, and compare against BBW [Jacobson et al. 2011] as implemented in Houdini 20.5 [SideFX 2025]. Each of the models was reposed in a T-pose, with legs spread. This can be done with any suitable method to smoothly separate the limbs into a specific pose like Laplacian mesh editing [Sorkine et al. 2004] or as-rigid-as-possible deformation [Sorkine and Alexa 2007]. For convenience, we used a different heuristic of deforming the character mesh using temporarily-transferred skinning weights from a fitted pre-skinned template. Although not strictly required, this ensures minimal self-intersections between the arms and torso and between the legs, producing a tetrahedralization with the fewest pruned intersecting triangles (required for Houdini’s tetrahedralizer), giving the best quality mesh and thus optimal biharmonic weights. This pose is also ideal for spatial weight methods [Li et al. 2024; Lin et al. 2022; Saito et al. 2021] like our approach, since it avoids significant weight contributions between adjacent limbs. In Fig. 13 we show the same pose for all skinned characters, and indicate where the method failed due to poor mesh quality (failed tetrahedralization). Notably, biharmonic weight computation failed on several characters, whereas our approach successfully computed weights for all. Furthermore, our method is able to produce good quality deformation while enforcing sparsity, which is especially noticeable for larger models with vertices far from the skeleton. For most other characters where biharmonic weight computation was successful and produced reasonably sparse fields, we observe comparable weight quality to our method.

*Comparison case study.* In Fig. 7, we compare different approaches for computing weights on a single bear character. Recall that Eq. 3

can be simplified to  $w(\mathbf{x}; S_j) = 1/d(\mathbf{x}; P_j)^{r_j}$ , which reduces SkinCells to a proximity-based method if all other parameters are fixed,  $t_{j,k}$  set to 0,  $F$  set to identity reducing to a Euclidean distance, and cell sites placed along skeleton bones. Setting the falloff  $r_j = 4$  results in the deformation shown in Fig. 7a, which exhibits significant artifacts. We can optimize just the falloff by minimizing the loss Eq. 7 over  $r_j$ , which produces the smooth result in Fig. 7b. While this case produces a compelling result, the deformation can exhibit volume loss for complex geometries as further investigated in the *Ablations* section below. Out-of-the-box BBW algorithm produces tearing artifacts when weights are clamped to the largest 4 as shown in Fig. 7c. However, this can be mitigated using compression (or sparsification) algorithms [Landreneau and Schaefer 2010; Le and Deng 2013] by optimizing per-vertex weights to be sparse. In Fig. 7d, we used the same loss from Eq. 7, to produce a smooth result, however regardless of the optimization technique, this approach struggles to resolve local minima when the weights are not initially sufficiently sparse. The full SkinCells approach in Fig. 7e generates a good quality result satisfying sparsity and smoothness, and it converges approximately 5x faster thanks to the abundance of tunable parameters available to SkinCells beyond just falloff.

*Ablations.* We further investigate the limitations of reducing SkinCells to optimize only the falloff as described in the previous paragraph. In the top row of Fig. 8 we highlight that the falloff-only optimization fails to capture the wrist bend since weights behave isometrically and so are not able to better fit the underlying geometry to minimize deformation artifacts. In the bottom row of Fig. 8 we highlight a few visible artifacts on another character demonstrating apparent volume loss in the muzzle and elbow, as well as extraneous deformation of the cape. In Fig. 9 we show that solely applying the sparse control to the falloff-only setup by employing Eq. 3 but still keeping other parameters fixed, we are able to recover reasonable quality weights. Here, the sparsity control allows the model to selectively prune contributions between regions without relying solely on  $r_j$ , which affects falloff equally in all directions. In this case, the full SkinCells method converges 3.5x faster to a result shown in Fig. 9c maintaining good quality deformation.

*Cloth skinning.* High-quality skinning weights are crucial for garments like loose clothing and long dresses, where disturbing artifacts are easily identified. Long dresses and skirts often suffer from abrupt splitting along the middle due to ambiguous leg mapping or frequent body intersections. To address this, we add a collision penalty term to the total loss (Eq. 7) [Stuyck et al. 2025], reducing body-clothing intersections. Our method produces noticeably less garment stretching compared to a proximity-based method as shown in Fig. 11. The proximity-based approach is implemented by identifying the  $l$ -nearest bones for each vertex, then assigning weights to these bones based on a distance  $d$  with a falloff of  $1/d^{3.5}$ , and finally normalizing the assigned weights to ensure they sum up to 1. We also compare against robust skinning weight transfer (RSWT) [Abdrashitov et al. 2023] where pre-determined weights on the body are used to drive the clothing. Compared to RSWT, our method is able to better resolve intersections with the body, and allow the cloth to follow a dedicated skirt rig.

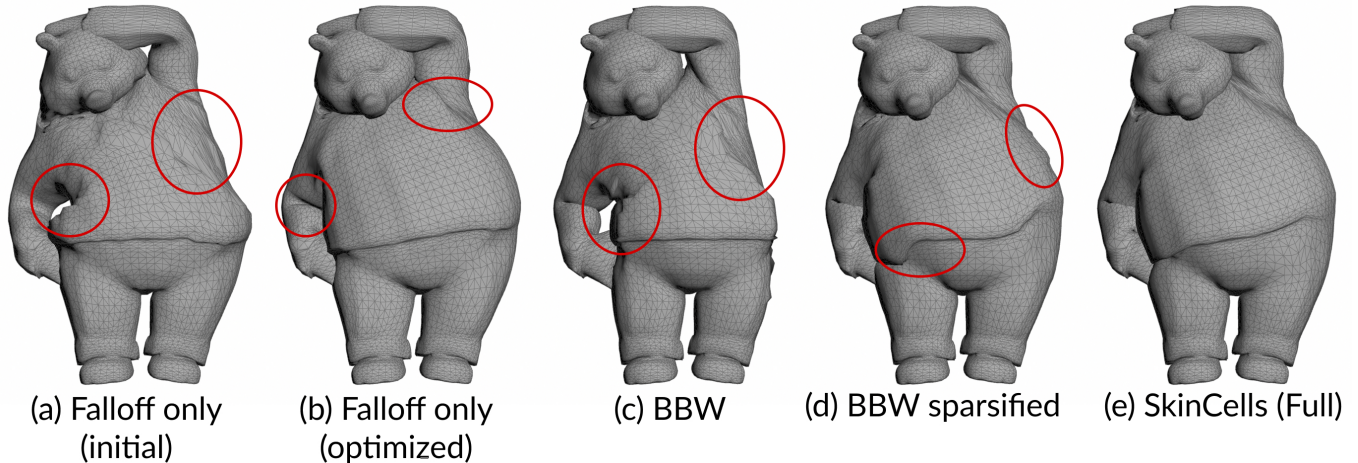


Fig. 7. We compare our method against others for optimizing skinning weights. In all cases bone influences are capped at 4 per vertex. The left two examples show the result of optimizing just the falloff coefficient  $r_j$ , while keeping all other parameters fixed. The figure marked with (initial) corresponds to the traditional proximity-based approach for computing skinning weights, showing significant artifacts. By optimizing just the falloff with our approach, we can already eliminate most sparsity artifacts. We also compare against the bounded biharmonic weights (BBW) method (c), which also shows artifacts since it lacks any sparsity controls. If we further optimize the BBW weights on each vertex to minimize the loss in Eq. 7 as shown in (d), we can eliminate some of the artifacts, although not all due to problematic local minima. Finally, the full SkinCells method produces a smooth result avoiding local minima and much more quickly than by optimizing falloff alone.

*Levels-of-detail and weight transfer.* Our method optimizes a spatially varying weight field for a garment mesh, which can then be applied to generate skinning weights for a higher-resolution, detailed mesh with small features like buttons or zippers. In Fig. 12, we demonstrate transferring weights from one skirt to a similar skirt. This example shows that standard proximity-based attribute transfer techniques fall short when aiming for high quality deformation. Using the weight field produced with our method, one can simply evaluate it at the locations of the vertices of the new mesh to produce a smoother result. Another application of this feature is automatically skinning meshes with varying levels-of-detail, where a single optimization is sufficient to provide weights for all levels. In Fig. 10, we show the optimization result using the mesh labeled “Original” with 9k vertices applied to a coarser mesh (left) and finer meshes (right), showing no visible skinning artifacts.

## 5 Discussion

In early experiments, we used a multi-layer perceptron (MLP) to generate the weight field similar to existing popular approaches. However, we found that MLPs could not reproduce the sparsity needed to avoid artifacts after clamping to a specified number of bones per vertex, even if minimizing  $\mathcal{L}_{sp}$ . This originally inspired the development of SkinCells, which is substantially more compact than a comparable MLP and uses intuitive parameters that allow for effective initialization, thus reducing optimization time.

Another simple alternative to SkinCells is optimizing weights on the vertices of meshes directly, however we found that such methods are less flexible and tend to converge to nearby local minima, thus struggling to make improvements on poor initializations.

## 6 Limitations and Future Work

*Canonical pose.* The Voronoi structure we use binds contiguous sections of space to the same bones, meaning that two points closer to one set of Voronoi sites than another will bind to the same bone. This being defined in 3D canonical space (as opposed to perhaps texture space) allows the algorithm to naturally bind surface elements that are close together to a similar set of bones. While generally this is desired, in some cases it can cause difficulties in distinguishing distinct parts of the body that are close together in canonical space. This is a well known limitation for any method that defines weight fields in canonical 3D space [Bhatnagar et al. 2020; Li et al. 2024; Lin et al. 2022; Saito et al. 2021], and the recommended solution is to reconfigure the canonical representation to have large gaps between limbs and digits (e.g. using a T-pose with legs spread forming an “A”). While this can be more challenging for fantastical characters and garments, we expect that an erosion algorithm to deform the geometry until all parts are well separated could help.

*Self-contact.* Our method does not account for self-contact when optimizing the skinning weights for garments. While self-contact can substantially improve the appearance of clothing in simulation, skinning is typically constrained to very few degrees of freedom that is usually insufficient to resolve self-intersections.

*Artist control.* While we designed our method to be fully automatic to enable automatic asset generation at scale, we acknowledge the benefit of optionally providing user-control to the generated results. Currently, one can manipulate the result by modifying the parameters associated with the optimization procedure, in the future we plan to leverage artist-painted weight maps to guide the optimization, offering more refined control.

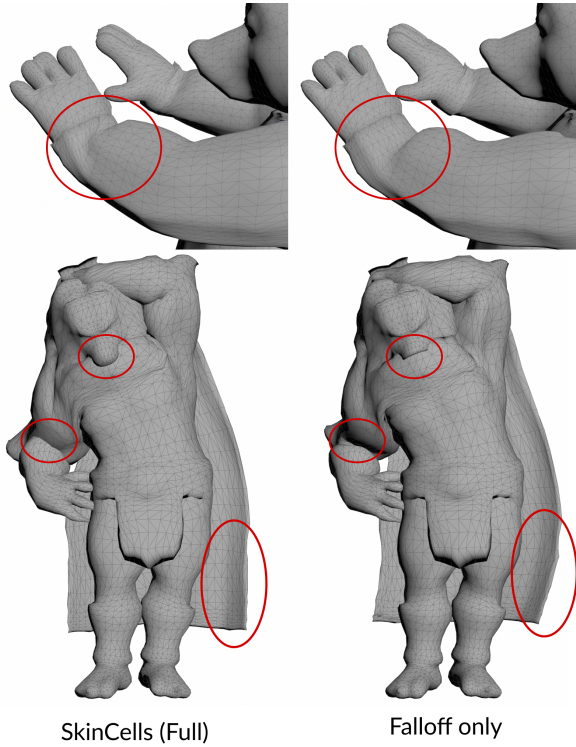


Fig. 8. Optimizing only the falloff can produce smooth results but without optimizing the location and shape of the cells, the field may exhibit various deformation artifacts if the underlying skeleton is not sufficiently expressive. The additional parameters in SkinCells can compensate for limited rigging as shown on the right.

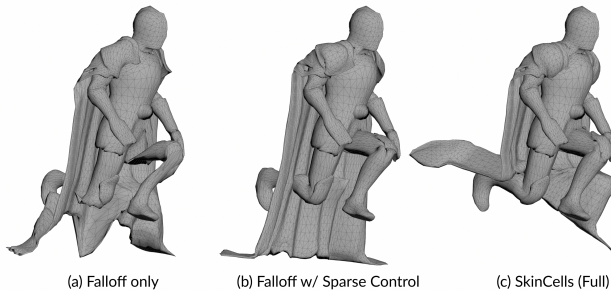


Fig. 9. The knight character is a particularly difficult example for skinning since the cape has no dedicated rig. As a result, without additional controls the optimization fails to find a suitable set of falloff coefficients to minimize the loss (a). Just adding the sparsity control in the numerator of Eq. 3 can already help exclude the cape from being influenced by the legs (b). The full SkinCells model retains this ability maintaining good quality deformation (c).

*3D representations.* The optimized skinning weight fields can be used to animate other 3D representations such as point clouds or volumetric primitives like Gaussian Splatting [Kerbl et al. 2023], but the optimization process relies on the mesh connectivity to

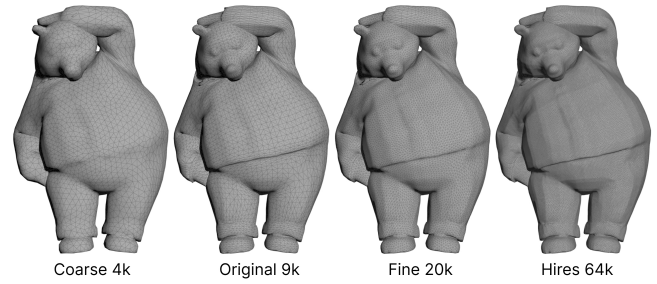


Fig. 10. The bear model in a stretching pose at 4 different resolutions showing one optimization result applied at various levels of detail. The optimization used the “Original” model, and the resulting weight field is evaluated at the vertices of the 4 different meshes in canonical pose to generate the final vertex weights. The labels indicate the approximate number of vertices in each mesh.

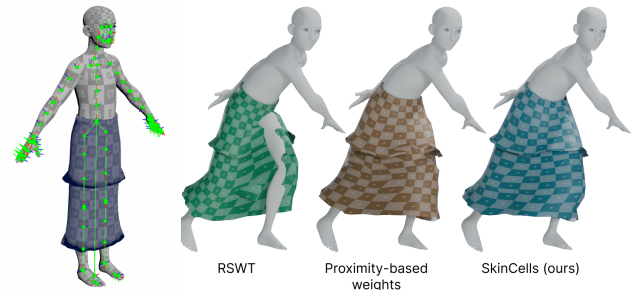


Fig. 11. We animate a skirt garment on a character with a dedicated skirt rig attached to the pelvis (left). Our optimization-based method significantly reduces excessive stretching, outperforming a standard proximity-based technique. In addition, we compare to RSWT [Abdrashitov et al. 2023] to show how weights transferred from the body fail to deform loose garments causing stretching and interpenetration.

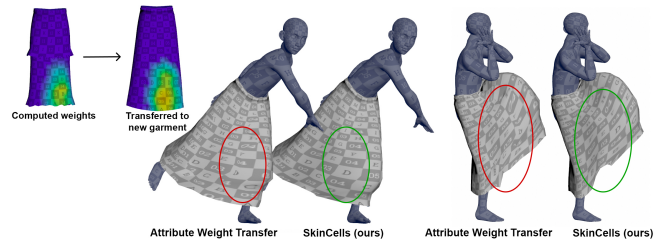


Fig. 12. We demonstrate how our method can aid in transferring weights between similar meshes. Here we transfer a set of precomputed weights from one skirt to another using Houdini (top left). We demonstrate that transferred weights can produce spurious stretches in the cloth, whereas applying our precomputed weight field to a similar garment can produce a smoother result.

evaluate the smoothness loss. We plan to explore alternatives to this loss to make our method even more general and support novel representations such as Gaussian avatars [Li et al. 2024] in future work.

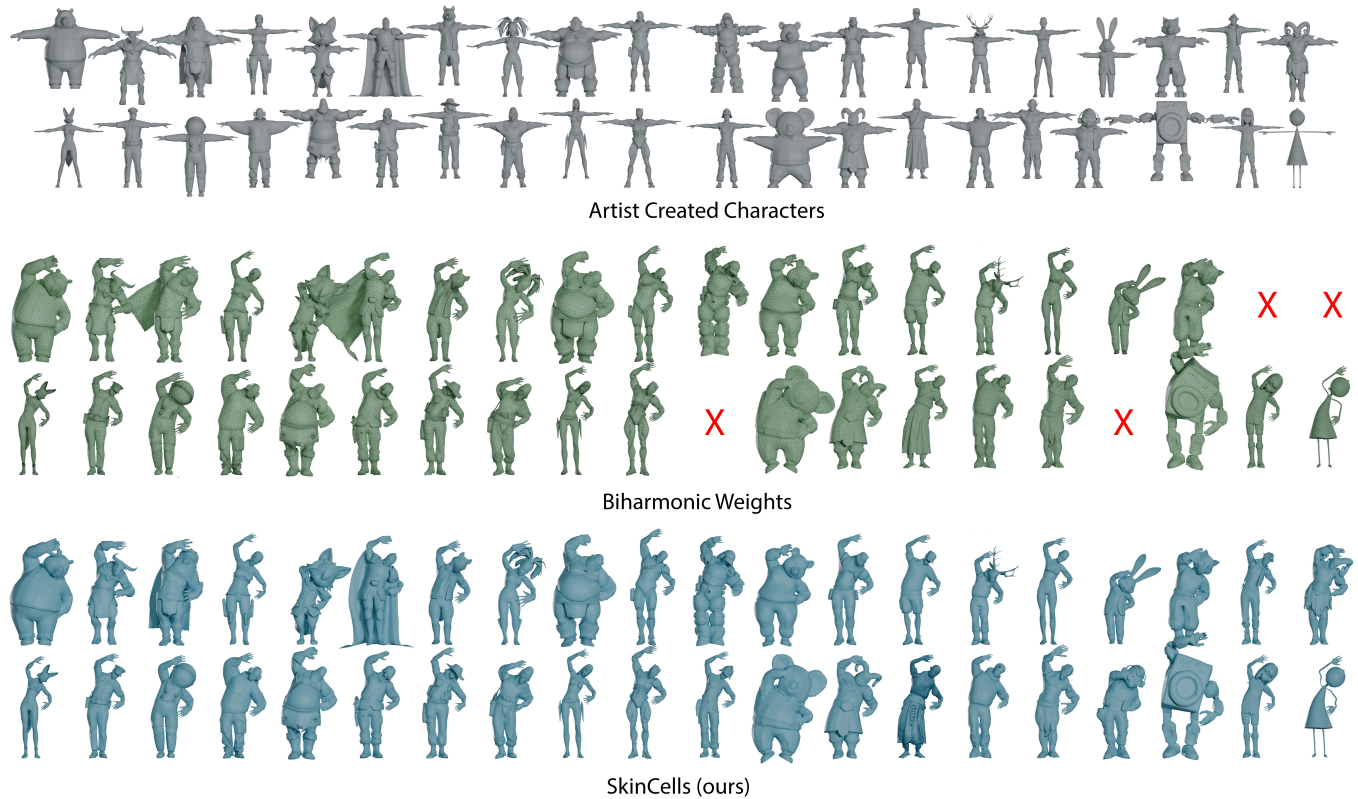


Fig. 13. 40 artist created characters (top) are skinned with 2 different methods. 36 out of 40 characters are skinned using bounded Biharmonic weights [Jacobson et al. 2011] (middle). 3 models fail to tetrahedralize and for 1 the biharmonic solve failed for all tried solve parameters. In contrast, all 40 characters were processed automatically and successfully with our method (bottom).

## 7 Conclusion

We introduce a fully automatic skinning weight optimization method that requires only the minimal amount of data necessary for skinning: a skeleton rig and character mesh. This approach eliminates the need for additional user input, enabling the efficient generation of optimal skinning weights for a vast number of virtual characters. Due to its fully automatic nature, our method is particularly well-suited to complement recent advances in automatic mesh generation. We propose a novel smoothness objective function that is minimized under automatically sampled poses, resulting in high-quality skinning weights. Our method is capable of enforcing a sparse set of bones influencing each vertex and our spatial nature for the weight definition allows for direct application to all resolutions in an LoD system. Through comprehensive evaluations, we demonstrate that our approach provides a robust solution to creating high quality skinning weights.

## Acknowledgements

We would like to thank Petr Kadlecek for his assistance with generating and formatting assets, and Edith Tretschk for her valuable feedback on neural methods as well as her help with implementation and code optimization. We are grateful to Nicky He for sourcing

motions and poses used in the early stages of training, and to Yu Ju (Edwin) Chen for insightful discussions on numerical methods and for narrating the supplemental video. Special thanks go to Rob Stratton for creating the manual skinning baselines for the initial skirt assets, Nicholas Burkard for helping with technical direction, and Gabriele Pellegrini for providing both art feedback and character skinning baselines. We also thank Anthony Yon for creating the skinning for the washing machine example, and Carlos Aliaga for his help in setting up rendered scenes.

## References

- Rinat Abdrashitov, Kim Raichstat, Jared Monsen, and David Hill. 2023. Robust Skin Weights Transfer via Weight Inpainting. In *SIGGRAPH Asia 2023 Technical Communications* (Sydney, NSW, Australia) (SA '23). Association for Computing Machinery, New York, NY, USA, Article 25, 4 pages. doi:10.1145/3610543.3626180
- Carlos Aliaga, Carol O'Sullivan, Diego Gutierrez, and Rasmus Tamstorf. 2015. Sackcloth or silk? the impact of appearance vs dynamics on the perception of animated cloth. In *Proceedings of the ACM SIGGRAPH Symposium on Applied Perception* (Tübingen, Germany) (SAP '15). Association for Computing Machinery, New York, NY, USA, 41–46. doi:10.1145/2804408.2804412
- Brett Allen, Brian Curless, Zoran Popović, and Aaron Hertzmann. 2006. Learning a correlated model of identity and pose-dependent body shape variation for real-time synthesis. In *Proceedings of the 2006 ACM SIGGRAPH/Eurographics symposium on Computer animation*. Citeseer, 147–156.
- Seungbae Bang and Sung-Hee Lee. 2018. Spline Interface for Intuitive Skinning Weight Editing. *ACM Transactions on Graphics (TOG)* 37, 5 (2018), 174.

- David Baraff and Andrew Witkin. 1998. Large steps in cloth simulation. In *Proceedings of the 25th Annual Conference on Computer Graphics and Interactive Techniques (SIGGRAPH '98)*. Association for Computing Machinery, New York, NY, USA, 43–54. doi:10.1145/280814.280821
- Ilya Baran and Jovan Popović. 2007. Automatic rigging and animation of 3D characters. *ACM Trans. Graph.* 26, 3 (July 2007), 72–es. doi:10.1145/1276377.1276467
- Otman Benchekroun, Jiayi Eris Zhang, Siddhartha Chaudhuri, Eitan Grinspun, Yi Zhou, and Alec Jacobson. 2023. Fast Complementary Dynamics via Skinning Eigenmodes. *ACM Trans. Graph.* 42, 4, Article 106 (July 2023), 21 pages. doi:10.1145/3592404
- Hugo Bertiche, Meysam Madadi, and Sergio Escalera. 2022. Neural Cloth Simulation. *ACM Trans. Graph.* 41, 6, Article 220 (nov 2022), 14 pages. doi:10.1145/3550454.3555491
- Bharat Lal Bhatnagar, Cristian Sminchisescu, Christian Theobalt, and Gerard Pons-Moll. 2020. LoopReg: Self-supervised Learning of Implicit Surface Correspondences, Pose and Shape for 3D Human Mesh Registration. In *Advances in Neural Information Processing Systems (NeurIPS)*.
- Ziyuan Cao and Tomohiko Mukai. 2024. Skeleton-Aware Skin Weight Transfer for Helper Joint Rigs.. In *Eurographics (Short Papers)*.
- Kwang-Jin Choi and Hyeong-Seok Ko. 2002. Stable but responsive cloth. *ACM Transactions on Graphics (TOG)* 21, 3 (2002), 604–611.
- Rich Diamant and Judd Simantov. 2010. Uncharted 2 Character Pipeline: An in-depth look at the creation of U2's characters. In *Game Developers Conference (GDC)*. [https://media.gdcvault.com/doi/pdf/10/slides/simantov\\_judd\\_uncharted2\\_character\\_pipeline.pdf](https://media.gdcvault.com/doi/pdf/10/slides/simantov_judd_uncharted2_character_pipeline.pdf) Slide 14: "3-5 influences per vertex - more than this becomes unmanageable".
- Olivier Dionne and Martin de Lasa. 2013. Geodesic Voxel Binding for Production Character Meshes. In *Eurographics/ ACM SIGGRAPH Symposium on Computer Animation*, Theodore Kim and Robert Sumner (Eds.). ACM SIGGRAPH / Eurographics Association. doi:10.1145/2485895.2485919
- Ana Dodik, Vincent Sitzmann, Justin Solomon, and Oded Stein. 2025. Robust Biharmonic Skinning Using Geometric Fields. *ACM Trans. Graph.* 45, 2, Article 14 (Dec. 2025), 18 pages. doi:10.1145/3771928
- Fan Feng, Shiyong Xiong, Ziyue Liu, Zangyueyang Xian, Yuqing Zhou, Hiroki Kobayashi, Atsushi Kawamoto, Tsuyoshi Nomura, and Bo Zhu. 2023. Cellular topology optimization on differentiable Voronoi diagrams. *Internat. J. Numer. Methods Engrg.* 124, 1 (2023), 282–304. doi:10.1002/nme.7121 arXiv:<https://onlinelibrary.wiley.com/doi/pdf/10.1002/nme.7121>
- Will Gao, Dilin Wang, Yuchen Fan, Aljaz Bozic, Tuur Stuyck, Zhengxin Li, Zhao Dong, Rakesh Ranjan, and Nikolaos Sarafianos. 2025. 3D Mesh Editing using Masked LRM. In *Proceedings of the IEEE/CVF International Conference on Computer Vision (ICCV)*. 7154–7165.
- Zhiyang Guo, Jinxu Xiang, Kai Ma, Wengang Zhou, Houqiang Li, and Ran Zhang. 2025. Make-It-Animateable: An Efficient Framework for Authoring Animation-Ready 3D Characters. In *Proceedings of the IEEE/CVF Conference on Computer Vision and Pattern Recognition (CVPR)*.
- Oshri Halimi, Tuur Stuyck, Donglai Xiang, Timur M Bagautdinov, He Wen, Ron Kimmel, Takaaki Shiratori, Chenglei Wu, Yaser Sheikh, and Fabian Prada. 2022. Pattern-Based Cloth Registration and Sparse-View Animation. *ACM Trans. Graph.* 41, 6 (2022), 196–1.
- Philipp Herholz, Felix Haase, and Marc Alexa. 2017. Diffusion Diagrams: Voronoi Cells and Centroids from Diffusion. *Computer Graphics Forum* 36, 2 (2017), 163–175. doi:10.1111/cgf.13116 arXiv:<https://onlinelibrary.wiley.com/doi/pdf/10.1111/cgf.13116>
- Peter J Huber. 1992. Robust estimation of a location parameter. In *Breakthroughs in statistics: Methodology and distribution*. Springer, 492–518.
- Alec Jacobson, Ilya Baran, Jovan Popović, and Olga Sorkine. 2011. Bounded biharmonic weights for real-time deformation. *ACM Trans. Graph.* 30, 4, Article 78 (July 2011), 8 pages. doi:10.1145/2010324.1964973
- Alec Jacobson, Zhigang Deng, Ladislav Kavan, and JP Lewis. 2014. Skinning: Real-time Shape Deformation. In *ACM SIGGRAPH 2014 Courses*.
- Niranjan Kalyanasundaram, Damien Rohmer, and Victor Zordan. 2022. Acceleration Skinning: Kinematics-Driven Cartoon Effects for Articulated Characters. In *Graphics Interface 2022*. <https://openreview.net/forum?id=BhGL3eYVa9>
- Ladislav Kavan, Steven Collins, Jiří Žára, and Carol O'Sullivan. 2007. Skinning with dual quaternions. In *Proceedings of the 2007 Symposium on Interactive 3D Graphics and Games (Seattle, Washington) (I3D '07)*. Association for Computing Machinery, New York, NY, USA, 39–46. doi:10.1145/1230100.1230107
- Ladislav Kavan and Olga Sorkine. 2012. Elasticity-inspired deformers for character articulation. *ACM Trans. Graph.* 31, 6, Article 196 (Nov. 2012), 8 pages. doi:10.1145/2366145.2366215
- Bernhard Kerbl, Georgios Kopanas, Thomas Leimkühler, and George Drettakis. 2023. 3D Gaussian Splatting for Real-Time Radiance Field Rendering. *ACM Transactions on Graphics* 42, 4 (July 2023).
- Theodore Kim and David Eberle. 2022. Dynamic deformables: implementation and production practicalities (now with code!). In *ACM SIGGRAPH 2022 Courses*. 1–259.
- Martin Komaritzan and Mario Botsch. 2018. Projective Skinning. *Proc. ACM Comput. Graph. Interact. Tech.* 1, 1, Article 12 (July 2018), 19 pages. doi:10.1145/3203203
- Eric Landreneau and Scott Schaefer. 2010. Poisson-Based Weight Reduction of Animated Meshes. *Computer Graphics Forum* (2010). doi:10.1111/j.1467-8659.2010.01661.x
- Binh Le and Zhigang Deng. 2012. Smooth Skinning Decomposition with Rigid Bones. *ACM Trans. Graph.* 31, 6 (Dec. 2012), in press.
- Binh Huy Le and Zhigang Deng. 2013. Two-layer sparse compression of dense-weight blend skinning. *ACM Trans. Graph.* 32, 4, Article 124 (July 2013), 10 pages. doi:10.1145/2461912.2461949
- J. P. Lewis, Matt Corder, and Nickson Fong. 2000. Pose space deformation: a unified approach to shape interpolation and skeleton-driven deformation. In *Proceedings of the 27th Annual Conference on Computer Graphics and Interactive Techniques (SIGGRAPH '00)*. ACM Press/Addison-Wesley Publishing Co., USA, 165–172. doi:10.1145/344779.344862
- Zhe Li, Zerong Zheng, Lizhen Wang, and Yebin Liu. 2024. Animatable Gaussians: Learning Pose-dependent Gaussian Maps for High-fidelity Human Avatar Modeling. In *Proceedings of the IEEE/CVF Conference on Computer Vision and Pattern Recognition (CVPR)*.
- Siyu Lin, Hongwen Zhang, Zerong Zheng, Ruizhi Shao, and Yebin Liu. 2022. Learning Implicit Templates for Point-Based Clothed Human Modeling. In *ECCV*.
- Isabella Liu, Zhan Xu, Wang Yifan, Hao Tan, Zexiang Xu, Xiaolong Wang, Hao Su, and Zifan Shi. 2025. RigAnything: Template-Free Autoregressive Rigging for Diverse 3D Assets. *ACM Trans. Graph.* 44, 4, Article 122 (July 2025), 12 pages. doi:10.1145/3731149
- Lijuan Liu, Youyi Zheng, Di Tang, Yi Yuan, Changjie Fan, and Kun Zhou. 2019. NeuroSkinning: automatic skin binding for production characters with deep graph networks. *ACM Trans. Graph.* 38, 4, Article 114 (July 2019), 12 pages. doi:10.1145/3306346.3322969
- Jing Ma, Jituo Li, and Dongliang Zhang. 2024. EasySkinning: Target-oriented skinning by mesh contraction and curve editing. *Computers & Graphics* 124 (2024), 104049. doi:10.1016/j.cag.2024.104049
- Miles Macklin and Matthias Muller. 2021. A Constraint-based Formulation of Stable Neo-Hookean Materials. In *Proceedings of the 14th ACM SIGGRAPH Conference on Motion, Interaction and Games (Virtual Event, Switzerland) (MIG '21)*. Association for Computing Machinery, New York, NY, USA, Article 12, 7 pages. doi:10.1145/3487983.3488289
- N. Magnenat-Thalmann, R. Laperrière, and D. Thalmann. 1989. Joint-dependent local deformations for hand animation and object grasping. In *Proceedings on Graphics Interface '88* (Edmonton, Alberta, Canada). Canadian Information Processing Society, CAN, 26–33.
- Joe Mancewicz, Matt L. Derksen, Hans Rijkema, and Cyrus A. Wilson. 2014. Delta Mush: smoothing deformations while preserving detail. In *Proceedings of the Fourth Symposium on Digital Production (Vancouver, British Columbia, Canada) (DigiPro '14)*. Association for Computing Machinery, New York, NY, USA, 7–11. doi:10.1145/2633374.2633376
- Vismay Modi, Nicholas Sharp, Or Perel, Shinjiro Sueda, and David I. W. Levin. 2024. Simplicitis: Mesh-Free, Geometry-Agnostic Elastic Simulation. *ACM Trans. Graph.* 43, 4, Article 117 (July 2024), 11 pages. doi:10.1145/3658184
- Albert Mosella-Montoro and Javier Ruiz-Hidalgo. 2022. SkinningNet: Two-Stream Graph Convolutional Neural Network for Skinning Prediction of Synthetic Characters. In *CVPR - CVF/IEEE Conference on Computer Vision and Pattern Recognition*.
- Damien Rohmer, Marco Tarini, Niranjan Kalyanasundaram, Faezeh Moshfeghifar, Marie-Paule Cani, and Victor Zordan. 2021. Velocity Skinning for Real-time Stylized Skeletal Animation. In *Computer Graphics Forum*, Vol. 40. Wiley Online Library, 549–561.
- Shunsuke Saito, Jinlong Yang, Qianli Ma, and Michael J. Black. 2021. SCANimate: Weakly Supervised Learning of Skinned Clothed Avatar Networks. In *Proceedings IEEE/CVF Conf. on Computer Vision and Pattern Recognition (CVPR)*.
- Igor Santesteban, Miguel A. Otaduy, and Dan Casas. 2019. Learning-Based Animation of Clothing for Virtual Try-On. *Computer Graphics Forum* 38, 2 (2019), 355–366. doi:10.1111/cgf.13643 arXiv:<https://onlinelibrary.wiley.com/doi/pdf/10.1111/cgf.13643>
- Igor Santesteban, Miguel A. Otaduy, and Dan Casas. 2022. SNUG: Self-Supervised Neural Dynamic Garments. In *2022 IEEE/CVF Conference on Computer Vision and Pattern Recognition (CVPR)*. 8130–8140. doi:10.1109/CVPR52688.2022.00797
- Igor Santesteban, Nils Thurey, Miguel A Otaduy, and Dan Casas. 2021. Self-supervised Collision Handling via Generative 3D Garment Models for Virtual Try-On. In *2021 IEEE/CVF Conference on Computer Vision and Pattern Recognition (CVPR)*. 11763–11773.
- Nikolaos Sarafianos, Tuur Stuyck, Xiaoyu Xiang, Yilei Li, Jovan Popovic, and Rakesh Ranjan. 2025. Garment3DGen: 3D Garment Stylization and Texture Generation. In *3DV*.
- SideFX. 2025. Houdini. <https://www.sidefx.com>. Version 20.5, 3D Animation and VFX Software.
- Breannan Smith, Fernando De Goes, and Theodore Kim. 2018. Stable neo-hookean flesh simulation. *ACM Transactions on Graphics (TOG)* 37, 2 (2018), 1–15.
- Chaoyue Song, Jianfeng Zhang, Xiu Li, Fan Yang, Yiwen Chen, Zhongcong Xu, Jun Hao Liew, Xiaoyang Guo, Fayao Liu, Jiashi Feng, and Guosheng Lin. 2025. MagicArticulate: Make Your 3D Models Articulation-Ready. In *Proceedings of the Computer*

- Vision and Pattern Recognition Conference (CVPR)*. 15998–16007.
- Olga Sorkine and Marc Alexa. 2007. As-rigid-as-possible surface modeling. In *Proceedings of the Fifth Eurographics Symposium on Geometry Processing (Barcelona, Spain) (SGP '07)*. Eurographics Association, Goslar, DEU, 109–116.
- O. Sorkine, D. Cohen-Or, Y. Lipman, M. Alexa, C. Rössl, and H.-P. Seidel. 2004. Laplacian surface editing (*SGP '04*). Association for Computing Machinery, New York, NY, USA, 175–184. doi:10.1145/1057432.1057456
- Tuur Stuyck. 2022. *Cloth simulation for computer graphics*. Springer Nature.
- Tuur Stuyck, Gene Wei-Chin Lin, Egor Larionov, Hsiao-yu Chen, Aljaz Bozic, Nikolaos Sarafianos, and Doug Roble. 2025. Quaffure: Real-Time Quasi-Static Neural Hair Simulation. In *Proceedings of the IEEE/CVF Conference on Computer Vision and Pattern Recognition (CVPR)*. 239–249.
- J.-M. Thiery and E. Eisemann. 2018. ARAPLBS: Robust and Efficient Elasticity-Based Optimization of Weights and Skeleton Joints for Linear Blend Skinning with Parametrized Bones. *Computer Graphics Forum* 37, 1 (2018), 32–44. doi:10.1111/cgf.13161 arXiv:https://onlinelibrary.wiley.com/doi/pdf/10.1111/cgf.13161
- Bohan Wang, Mianlun Zheng, and Jernej Barbič. 2020. Adjustable Constrained Soft-Tissue Dynamics. In *Computer Graphics Forum*, Vol. 39. Wiley Online Library, 69–79.
- Yu Wang and Justin Solomon. 2021. Fast quasi-harmonic weights for geometric data interpolation. *ACM Trans. Graph.* 40, 4, Article 73 (July 2021), 15 pages. doi:10.1145/3450626.3459801
- Rich Wareham and Joan Lasenby. 2008. Bone Glow: An Improved Method for the Assignment of Weights for Mesh Deformation. In *Proceedings of the 5th International Conference on Articulated Motion and Deformable Objects (Port d'Andratx, Mallorca, Spain) (AMDO '08)*. Springer-Verlag, Berlin, Heidelberg, 63–71. doi:10.1007/978-3-540-70517-8\_7
- Xinyue Wei, Kai Zhang, Sai Bi, Hao Tan, Fujun Luan, Valentin Deschaintre, Kalyan Sunkavalli, Hao Su, and Zexiang Xu. 2024. MeshLRM: Large Reconstruction Model for High-Quality Meshes. *arXiv preprint arXiv:2404.12385* (2024).
- Hongyi Xu and Jernej Barbič. 2016. Pose-space subspace dynamics. *ACM Transactions on Graphics (TOG)* 35, 4 (2016), 1–14.
- Hongyi Xu, Eduard Gabriel Bazavan, Andrei Zanfir, William T Freeman, Rahul Sunkavalli, and Cristian Sminchisescu. 2020a. Ghum & ghuml: Generative 3d human shape and articulated pose models. In *Proceedings of the IEEE/CVF Conference on Computer Vision and Pattern Recognition*. 6184–6193.
- Zhan Xu, Yang Zhou, Evangelos Kalogerakis, Chris Landreth, and Karan Singh. 2020b. RigNet: Neural Rigging for Articulated Characters. *ACM Trans. on Graphics* 39 (2020).
- Ze Yang, Shenlong Wang, Sivabalan Manivasagam, Zeng Huang, Wei-Chiu Ma, Xinchun Yan, Ersin Yumer, and Raquel Urtasun. 2021. S3: Neural shape, skeleton, and skinning fields for 3d human modeling. In *Proceedings of the IEEE/CVF conference on computer vision and pattern recognition*. 13284–13293.
- Jiayi Eris Zhang, Seungbae Bang, David I.W. Levin, and Alec Jacobson. 2020. Complementary Dynamics. *ACM Transactions on Graphics* (2020).
- Longwen Zhang, Ziyu Wang, Qixuan Zhang, Qiwei Qiu, Anqi Pang, Haoran Jiang, Wei Yang, Lan Xu, and Jingyi Yu. 2024. CLAY: A Controllable Large-scale Generative Model for Creating High-quality 3D Assets. *ACM Transactions on Graphics (TOG)* 43, 4 (2024), 1–20.
- Mianlun Zheng and Jernej Barbič. 2024. Multi-Resolution Real-Time Deep Pose-Space Deformation. *ACM Transactions on Graphics (TOG)* 43, 6 (2024), 1–11.